SUPPLEMENTAL MATERIAL

Quantum magnetism and topological superconductivity in Yu-Shiba-Rusinov chains

Jacob F. Steiner, Christophe Mora, Katharina J. Franke, Felix von Oppen

I. MAPPING TO EXTENDED $t-J$ MODEL

In this section, we present details of the mapping from the original model in Eq. (1) to the extended $t-J$ model in Eq. (2), which is valid for impurities with spin $S=1/2$ for $\Delta, V, K \to \infty$ at finite E_{YSR}. We will first discuss the mapping for a single impurity (Sec. I A) and then extend it to a chain of impurities (Sec. I B). Finally, we include spin-orbit coupling (Sec. I C) and consider the spectral function (Sec. I D) at the level of the extended $t-J$ model.

We begin by briefly summarizing the main ideas. As described in the main text, the model in Eq. (1) has three low-energy states for each site: the singlet state $|0\rangle = \frac{1}{\sqrt{2}}(|\Uparrow\downarrow\rangle - |\Downarrow\uparrow\rangle)$ corresponding to a screened impurity spin, and the BCS-paired doublet $|\pm\rangle = \left|S^z = \pm\frac{1}{2}\right\rangle \otimes |\mathrm{BCS}\rangle$ describing a free impurity spin. This resembles a single spinful electronic orbital with infinite on-site repulsion, when considering the spin singlet $|0\rangle$ as the empty orbital and the spin-up and spin-down states $|\pm\rangle$ of the unscreened doublet as the singly-occupied orbital. We project out the doubly-occupied site, which has no analog in the original model. This constraint is the key feature of t-J models. Formally, it can be enforced by including an on-site potential $U \to \infty$.

The fermionic operators d_σ for this orbital are introduced as follows. The singlet involves the singly-occupied states $|\sigma\rangle = c_\sigma^\dagger|\mathrm{vac}\rangle$, which can also be obtained from the BCS ground state using the Bogoliubov operators γ_σ through $|\sigma\rangle = \gamma_\sigma^\dagger|\mathrm{BCS}\rangle$. The free-spin states (involving $|\mathrm{BCS}\rangle$ as the electronic state) are thus obtained from the singlet by annihilating a quasiparticle, and the new fermion creation operators $d_\sigma^\dagger$ essentially correspond to the quasiparticle annihilation operators $\gamma_{\bar\sigma}$. Taking into account the detailed singlet state, we find (restoring the site index)

$$\gamma_{j,\sigma} = u c_{j,\sigma} + \sigma v c_{j,\bar\sigma}^\dagger \sim \sigma \frac{(-1)^j}{\sqrt{2}} d_{j,\bar\sigma}^\dagger. \tag{S1}$$

Here, we use $\sim$ rather than an equality since strictly speaking, the two operators are equivalent only when projecting to the low-energy subspace. Note that there is no correspondence between the high energy states ($E \sim \Delta, K, V$) of the original model and the doubly-occupied orbital ($E \sim U$), see also Table I. Importantly, the d-fermions of the extended $t-J$ model therefore correspond to Bogoliubov operators of the original Hamiltonian. This implies that the electron spectral function measured in tunneling experiments is not identical to the spectral function of the extended $t-J$ model. Instead, it involves anomalous terms when written in terms of the d-fermions.

Below, we consider the mapping as well as the physical spectral function in detail.

A. Single magnetic impurity

We first consider a single $S=1/2$ impurity coupled to a single-site superconductor as described by the Hamiltonian

$$H = \Delta\left(c_\uparrow^\dagger c_\downarrow^\dagger + \mathrm{h.c.}\right) + \sum_{\sigma\sigma'} c_\sigma^\dagger (V\delta_{\sigma\sigma'} + K\mathbf{S}\cdot\mathbf{s}_{\sigma\sigma'}) c_{\sigma'} \tag{S2}$$

and focus on YSR states in the vicinity of the band center. We can formally implement this limit by taking the exchange coupling K (assumed isotropic), the gap Δ, and the potential scattering V of the substrate to infinity, while keeping the energy of the Yu-Shiba-Rusinov (YSR) state and the particle-hole asymmetry V/Δ fixed.

The Hamiltonian H conserves fermion parity. Without coupling to the impurity spin, the even-fermion-parity eigenstates and eigenenergies of the single-site superconductor are

$$|\mathrm{BCS}\rangle = u\,|\mathrm{vac}\rangle + v\,|{\downarrow\uparrow}\rangle\,,\ E_{\mathrm{BCS}} = V - \sqrt{\Delta^2+V^2}, \tag{S3a}$$

$$\left|\overline{\mathrm{BCS}}\right\rangle = v\,|\mathrm{vac}\rangle - u\,|{\downarrow\uparrow}\rangle\,,\ E_{\overline{\mathrm{BCS}}} = V + \sqrt{\Delta^2+V^2}. \tag{S3b}$$

Here, $|{\downarrow\uparrow}\rangle = c_\downarrow^\dagger c_\uparrow^\dagger|\mathrm{vac}\rangle$. (We reserve $|0\rangle$ for the singlet state.) $|\mathrm{BCS}\rangle$ denotes the BCS ground state and $\left|\overline{\mathrm{BCS}}\right\rangle$ the excited state with two Boguliubov quasiparticles. The odd-fermion-parity eigenstates

$$|\sigma\rangle = c_\sigma^\dagger\,|\mathrm{vac}\rangle = \gamma_\sigma^\dagger\,|\mathrm{BCS}\rangle\,,\ E_\sigma = V \tag{S4}$$

Original model			$t-J$ model		
$\sum_\sigma \gamma_\sigma^\dagger \gamma_\sigma$	high energy	low energy	low energy	high energy	$\sum_\sigma d_\sigma^\dagger d_\sigma$
2	$\left\|S^z, \overline{\mathrm{BCS}}\right\rangle$				
1	$\left\|\Uparrow\uparrow\right\rangle, \left\|\Downarrow\downarrow\right\rangle,$ $\left\|\Uparrow\downarrow\right\rangle + \left\|\Downarrow\uparrow\right\rangle$	$\left\|\Uparrow\downarrow\right\rangle - \left\|\Downarrow\uparrow\right\rangle$	$\left\|\mathrm{vac}\right\rangle_H$		0
0		$\left\|S^z, \mathrm{BCS}\right\rangle$	$\left\|\sigma\right\rangle_H$		1
				$\left\|\downarrow\uparrow\right\rangle_H$	2

Table I. Correspondence between the local Hilbert spaces for the original model (Eq. (S2); left) and the $t-J$ model (Eq. (S23); right). There is a direct correspondence between the low-energy states of both models (as indicated by the red arrows), but no such correspondence between the high-energy states that are effectively projected out in the limit considered. The correspondence of the low-energy states is guided by matching spin multiplicities. While the relation $\gamma_\sigma \sim d_{\bar\sigma}^\dagger$ has aspects of a particle-hole transformation, the fermion parities are different in the two models. The singlet state of the original model (odd fermion parity) corresponds to the vacuum state (even fermion parity) in the $t-J$ representation. Thus, the doubly occupied states of either model have no corresponding states in the other, see the outermost columns with the respective fermion numbers. (For the $t-J$ model, the doubly-occupied state exists only when implementing the projection through a Hubbard repulsion $U \to \infty$.)

can be either viewed as excited states with one Bogoliubov quasiparticle or as single-electron states unaffected by pairing. Here, we defined the Bogoliubov quasiparticle operators

$$\gamma_\uparrow^\dagger = u c_\uparrow^\dagger + v c_\downarrow, \;\; \gamma_\downarrow^\dagger = u c_\downarrow^\dagger - v c_\uparrow, \tag{S5}$$

with the electron and hole amplitudes

$$u = \sqrt{\frac{1}{2}\left(1 + \frac{V}{\sqrt{\Delta^2+V^2}}\right)}, \;\; v = \sqrt{\frac{1}{2}\left(1 - \frac{V}{\sqrt{\Delta^2+V^2}}\right)}. \tag{S6}$$

The electron and hole amplitudes are in general different as a result of the potential scattering V by the impurity.

The exchange interaction K couples the single-site superconductor to the impurity spin. Due to Eq. (S4), we can replace the electron operators c_σ in the exchange Hamiltonian by the corresponding Bogoliubov operators. Expressing the Hamiltonian of the single-site superconductor in terms of the Bogoliubov operators, we have

$$H = V + \sqrt{\Delta^2+V^2}\left(\sum_\sigma n_\sigma - 1\right) + \sum_{\sigma\sigma'} K \gamma_\sigma^\dagger \mathbf{S}\cdot\mathbf{s}_{\sigma\sigma'}\gamma_{\sigma'}, \tag{S7}$$

where $n_\sigma = \gamma_\sigma^\dagger\gamma_\sigma$. We can also write the exchange coupling in terms of spin raising and lowering operators, $\mathbf{S}\cdot\mathbf{s} = S^z s^z + \frac{1}{2}(S^+ s^- + S^- s^+)$. In the following, we will at times use the abbreviated notation

$$s^z = \frac{1}{2}\left(c_\uparrow^\dagger c_\uparrow - c_\downarrow^\dagger c_\downarrow\right) = \frac{1}{2}(n_\uparrow - n_\downarrow), \;\; s^+ = \left(s^-\right)^\dagger = c_\uparrow^\dagger c_\downarrow = \gamma_\uparrow^\dagger \gamma_\downarrow, \tag{S8}$$

which incorporates the fermion operators into $\mathbf{s}$. The even-fermion-parity sector is not affected by the exchange coupling as all corresponding matrix elements of $\mathbf{s}$ vanish. As a result, the even-fermion-parity states are doubly degenerate due to the unscreened impurity spin. This can also be viewed as a Kramers degeneracy. The ground states in the even-fermion-parity sector are thus

$$|\pm\rangle \equiv \left|S^z = \pm\frac{1}{2}, \mathrm{BCS}\right\rangle = \left|S^z = \pm\frac{1}{2}\right\rangle \otimes |\mathrm{BCS}\rangle \tag{S9}$$

with energy E_{BCS}. Within the odd-fermion-parity sector, the antiferromagnetic exchange couples the electron and impurity spins into a singlet ground state,

$$|0\rangle = \frac{1}{\sqrt{2}}(\left|\Uparrow\downarrow\right\rangle - \left|\Downarrow\uparrow\right\rangle), \;\; E_0 = V - \frac{3}{4}K. \tag{S10}$$

where $|S^z,\sigma\rangle = |S^z\rangle \otimes c_\sigma^\dagger |\text{vac}\rangle$. The excited triplet states have energy $V + K/4$. Comparing the ground-state energies of the even- and odd-fermion-parity ground states in Eqs. (S3a) and (S10), respectively, one concludes that there is a quantum phase transition between even- and odd-fermion-parity ground states when $E_{\text{BCS}} = E_0$, i.e., when

$$\frac{3}{4}K = \sqrt{\Delta^2 + V^2}. \tag{S11}$$

The energy difference between these ground states is the excitation energy of the Yu-Shiba-Rusinov state,

$$E_{\text{YSR}} = E_0 - E_{\text{BCS}} = \sqrt{\Delta^2 + V^2} - \frac{3}{4}K. \tag{S12}$$

We thus define E_{YSR} as positive when the impurity spin in unscreened in the ground state and as negative when the impurity is screened.

We now focus on the limit of K, Δ, and V large, keeping E_{YSR} and V/Δ fixed, thereby eliminating above-gap excitations (which are not properly described within the single-site model due to the lack of a quasiparticle continuum). Then, only the singlet state and the BCS states with unscreened impurity spin remain relevant for the low-energy physics. We can define the projector onto the low-energy subspace through

$$P = P_{\text{BCS}} + P_0, \text{ with } P_{\text{BCS}} = \sum_{\pm} |\pm\rangle\langle\pm|, \; P_0 = |0\rangle\langle 0|. \tag{S13}$$

The low-energy projected Hamiltonian is then

$$PHP = -E_{\text{YSR}} P_{\text{BCS}} + \left(V - \frac{3}{4}K\right)P. \tag{S14}$$

We proceed by investigating the action of the projected Bogoliubov operators $P\gamma_\sigma P$, $P\gamma_\sigma^\dagger P$ as well as PS^iP on the low-energy subspace. We will find that they satisfy the same algebra as the $t-J$ fermions (i.e., spinful electrons with the constraint that double occupancy is forbidden). Consider first the action of $P\gamma_\sigma P$ on the singlet,

$$P\gamma_\downarrow P|0\rangle = \frac{1}{\sqrt{2}}|+\rangle, \; P\gamma_\uparrow P|0\rangle = -\frac{1}{\sqrt{2}}|-\rangle. \tag{S15}$$

Thus, the states $|\pm\rangle$ are created from $|0\rangle$ by application of $P\gamma_{\downarrow/\uparrow}P$ (up to normalization). Similarly, we have

$$P\gamma_\sigma^\dagger P|\pm\rangle = \begin{cases} 0 \text{ if } \sigma = \pm \\ \frac{\bar{\sigma}}{\sqrt{2}}|0\rangle \text{ if } \sigma = \mp \end{cases}, \; P\gamma_\sigma^\dagger P|0\rangle = 0. \tag{S16}$$

Thus, $P\gamma_\sigma^\dagger P$ acts as annihilator for the excitations with $\pm = \bar{\sigma}$, while $|0\rangle$ acts as the vacuum. Finally, consider the action of $P\gamma_\sigma P$ on the already occupied $|\pm\rangle$,

$$P\gamma_\sigma P|\pm\rangle = 0. \tag{S17}$$

Following these observations, for $\sigma = \mp$ this corresponds to adding a second spin-σ electron into the already occupied state, which should indeed give 0. However, the above also implies $P\gamma_\uparrow P\gamma_\downarrow P|0\rangle = 0$, which corresponds to forbidden double occupation. This motivates the definition of new quasi-fermionic creation operators

$$\Gamma_\sigma^\dagger = \sigma\sqrt{2}P\gamma_{\bar{\sigma}}P, \tag{S18}$$

which create the states $|\pm = \sigma\rangle$ from $|0\rangle$. They satisfy

$$\Gamma_\sigma^\dagger\Gamma_\sigma^\dagger = 0 = \Gamma_\sigma\Gamma_\sigma. \tag{S19}$$

Due to the forbidden double occupation, these are not proper fermions. Their full anticommutation algebra on the low-energy subspace is given by

$$\left\{\Gamma_\uparrow, \Gamma_\uparrow^\dagger\right\}\begin{pmatrix}|0\rangle \\ |+\rangle \\ |-\rangle\end{pmatrix} = \begin{pmatrix}|0\rangle \\ |+\rangle \\ 0\end{pmatrix}, \; \left\{\Gamma_\downarrow, \Gamma_\downarrow^\dagger\right\}\begin{pmatrix}|0\rangle \\ |+\rangle \\ |-\rangle\end{pmatrix} = \begin{pmatrix}|0\rangle \\ 0 \\ |-\rangle\end{pmatrix}, \tag{S20a}$$

$$\left\{\Gamma_\downarrow, \Gamma_\uparrow^\dagger\right\}\begin{pmatrix}|0\rangle \\ |+\rangle \\ |-\rangle\end{pmatrix} = \begin{pmatrix}0 \\ 0 \\ |+\rangle\end{pmatrix}, \; \left\{\Gamma_\uparrow, \Gamma_\downarrow^\dagger\right\}\begin{pmatrix}|0\rangle \\ |+\rangle \\ |-\rangle\end{pmatrix} = \begin{pmatrix}0 \\ |-\rangle \\ 0\end{pmatrix}, \tag{S20b}$$

while

$$\left\{\Gamma_\uparrow^\dagger, \Gamma_\downarrow^\dagger\right\} = 0 = \{\Gamma_\uparrow, \Gamma_\downarrow\}. \tag{S20c}$$

We now show explicitly that these operators satisfy the same algebra as the $t-J$ fermions. To this end, consider a single site, infinite-U Hubbard model described by fermionic operators d_σ, with states $|\mathrm{vac_H}\rangle, |\sigma_\mathrm{H}\rangle = d_\sigma^\dagger |\mathrm{vac_H}\rangle$ and the doubly occupied $|{\downarrow\uparrow_\mathrm{H}}\rangle = d_\downarrow^\dagger d_\uparrow^\dagger |\mathrm{vac_H}\rangle$, as well as the projector onto the empty and singly-occupied states, $P_\mathrm{H} = 1 - |{\downarrow\uparrow_\mathrm{H}}\rangle\langle{\downarrow\uparrow_\mathrm{H}}|$. Note that, for sake of simplicity, in the main text no distinction is made between the Hilbert space of the original model and that of the Hubbard model. As above we define the projected quasi-fermion operators as

$$D_\sigma = P_\mathrm{H} d_\sigma P_\mathrm{H}. \tag{S21}$$

It is straightforward to check the anticommutation relations. As above

$$\left\{D_\uparrow, D_\uparrow^\dagger\right\} \begin{cases} |\mathrm{vac_H}\rangle \\ |{\uparrow_\mathrm{H}}\rangle \\ |{\downarrow_\mathrm{H}}\rangle \end{cases} = \begin{cases} |\mathrm{vac_H}\rangle \\ |{\uparrow_\mathrm{H}}\rangle \\ -P_\mathrm{H} d_\uparrow P_\mathrm{H} |{\downarrow\uparrow_\mathrm{H}}\rangle = 0 \end{cases}, \tag{S22a}$$

$$\left\{D_\downarrow, D_\downarrow^\dagger\right\} \begin{cases} |\mathrm{vac_H}\rangle \\ |{\uparrow_\mathrm{H}}\rangle \\ |{\downarrow_\mathrm{H}}\rangle \end{cases} = \begin{cases} |\mathrm{vac_H}\rangle \\ P_\mathrm{H} d_\downarrow P_\mathrm{H} |{\downarrow\uparrow_\mathrm{H}}\rangle = 0 \\ |{\downarrow_\mathrm{H}}\rangle \end{cases}, \tag{S22b}$$

$$\left\{D_\downarrow, D_\uparrow^\dagger\right\} \begin{cases} |\mathrm{vac_H}\rangle \\ |{\uparrow_\mathrm{H}}\rangle \\ |{\downarrow_\mathrm{H}}\rangle \end{cases} = \begin{cases} 0 \\ 0 \\ -P_\mathrm{H} D_\downarrow d_\mathrm{H} |{\downarrow\uparrow_\mathrm{H}}\rangle + |{\uparrow_\mathrm{H}}\rangle = |{\uparrow_\mathrm{H}}\rangle \end{cases}, \tag{S22c}$$

$$\left\{D_\uparrow, D_\downarrow^\dagger\right\} \begin{cases} |\mathrm{vac_H}\rangle \\ |{\uparrow_\mathrm{H}}\rangle \\ |{\downarrow_\mathrm{H}}\rangle \end{cases} = \begin{cases} 0 \\ P_\mathrm{H} d_\uparrow P_\mathrm{H} |{\downarrow\uparrow_\mathrm{H}}\rangle + |{\downarrow_\mathrm{H}}\rangle = |{\downarrow_\mathrm{H}}\rangle \\ 0 \end{cases}, \tag{S22d}$$

and

$$\left\{D_\uparrow^\dagger, D_\downarrow^\dagger\right\} = 0 = \{D_\uparrow, D_\downarrow\}. \tag{S22e}$$

Thus, the low-energy projected superconductor may be described using the infinite-U Hubbard model instead, with $\gamma_\sigma \sim -\sigma d_{\bar\sigma}^\dagger/\sqrt{2}$. As mentioned above, we introduce the $\sim$-symbol to mean equivalence at the level of the low-energy projected theory. The corresponding Hamiltonian is

$$H_\mathrm{H} = -E_\mathrm{YSR} \sum_\sigma d_\sigma^\dagger d_\sigma + V - \frac{3}{4}K + U d_\uparrow^\dagger d_\uparrow d_\downarrow^\dagger d_\downarrow,\ U \to \infty. \tag{S23}$$

The merits of this identification will become clear when considering chains in the next section. Table I shows a comparison of this $t-J$ (or infinite-U Hubbard) model to the original model Eq. (S2), highlighting that the equivalence holds only at the level of the low energy projected theory. In particular, we emphasize that the Hubbard potential U merely implements the projection and is not a physical parameter.

We have not yet discussed the low-energy projected spin operators PS^iP. They act like the spin operators associated with the d fermions,

$$S^z \sim \frac{1}{2}\sum_\sigma \sigma d_\sigma^\dagger d_\sigma,\ S^+ \sim d_\uparrow^\dagger d_\downarrow,\ S^- \sim d_\downarrow^\dagger d_\uparrow. \tag{S24}$$

To see this, we explicitly consider their action on the low-energy states,

$$PS^zP\,|0\rangle \propto P(|{\Uparrow\downarrow}\rangle + |{\Downarrow\uparrow}\rangle) = 0,\ PS^zP\,|\pm\rangle = \pm\frac{1}{2}\,|\pm\rangle\,, \tag{S25a}$$

$$PS^+P\,|0\rangle \propto P\,|{\Uparrow\uparrow}\rangle = 0,\ PS^\pm P\,|\pm\rangle = 0,\ PS^\mp P\,|\pm\rangle = |\mp\rangle\,. \tag{S25b}$$

B. Spin-$\frac{1}{2}$ chain

We now generalize to a chain of spin-$\frac{1}{2}$ impurities with isotropic exchange K and general RKKY interaction J (possibly including Dzyaloshinskii-Moriya interactions),

$$H = \sum_j \left[\Delta\Big(c^\dagger_{j,\uparrow} c^\dagger_{j,\downarrow} + \text{h.c.}\Big) + \sum_{\sigma\sigma'} c^\dagger_{j,\sigma}(V\delta_{\sigma\sigma'} + K\mathbf{S}_j \cdot \mathbf{s}_{\sigma\sigma'}) c_{j,\sigma'} - t\sum_\sigma \Big(c^\dagger_{j,\sigma} c_{j+1,\sigma} + \text{h.c.}\Big) + \mathbf{S}_j \cdot J \cdot \mathbf{S}_{j+1} \right]. \tag{S26}$$

Note that there is no single-ion anisotropy for spin-$\frac{1}{2}$ impurities.

We want to project this Hamiltonian to the low-energy subspace introduced in the previous section. As a first step, we rewrite the tunneling Hamiltonian in terms of Bogoliubov operators,

$$H_t = \sum_j \left[-t(u^2 - v^2) \sum_\sigma \Big(\gamma^\dagger_{j,\sigma}\gamma_{j+1,\sigma} + \text{h.c.}\Big) + 2tuv\Big(\gamma^\dagger_{j,\uparrow}\gamma^\dagger_{j+1,\downarrow} - \gamma^\dagger_{j,\downarrow}\gamma^\dagger_{j+1,\uparrow} + \text{h.c.}\Big)\right], \tag{S27}$$

and define the effective hopping and pairing amplitudes

$$\tilde{t} = \frac{t}{2}(u^2 - v^2) = \frac{tV}{2\sqrt{\Delta^2 + V^2}},\ \tilde{\Delta} = tuv = \frac{t\Delta}{2\sqrt{\Delta^2 + V^2}}. \tag{S28}$$

Next, we apply the projection

$$\mathcal{P} = \prod_j P_j, \tag{S29}$$

where P_j are the local projectors defined by Eq. (S13). We obtain

$$\begin{aligned}\mathcal{P}H\mathcal{P} = \mathcal{P}\sum_j \Bigg[&- E_{\text{YSR}} P_{j,\text{BCS}} + \left(V - \frac{3}{4}K\right)P_j - \tilde{t}\sum_\sigma \Big(\Gamma_{j,\sigma}\Gamma^\dagger_{j+1,\sigma} + \text{h.c.}\Big) \\ &+ \tilde{\Delta}(-\Gamma_{j,\downarrow}\Gamma_{j+1,\uparrow} + \Gamma_{j,\uparrow}\Gamma_{j+1,\downarrow} + \text{h.c.}) + P_j\mathbf{S}_j P_j \cdot J \cdot P_{j+1}\mathbf{S}_{j+1}P_{j+1}\Bigg]\mathcal{P},\end{aligned} \tag{S30}$$

in terms of the projected operators $\Gamma_{j,\sigma} = \sigma\sqrt{2}P_j\gamma^\dagger_{j,\bar{\sigma}}P_j$. As in the single-site case discussed in the previous section, the $\Gamma_{j,\sigma}$ have the same anticommutation algebra as $t-J$ fermions. The on-site algebra follows from the previous section. Furthermore, it is clear that $\{\Gamma_{j,\sigma}, \Gamma_{j',\sigma'}\} \propto P_j P_{j'}\{\gamma^\dagger_{j,\bar{\sigma}}, \gamma^\dagger_{j',\bar{\sigma}'}\}P'_j P_j = 0$ for $j \neq j'$ since $[P_j, P_{j'}] = 0$ and similarly for the anticommutator of creation and annihilation operators.

There is one more issue to account for to make the mapping exact. The new vacuum is a product of local singlet states, and therefore has odd local fermion parities. Similarly, the single-occupied sites actually have even local fermion parity. Thus, acting with $\Gamma^\dagger_j$ on a basis state, there is an overall minus sign equal to the parity of the number of singlets on sites $i < j$, i.e. of the number of "unoccupied" rather than "occupied" states. To make this precise, consider the action of $\Gamma_{j,\sigma}$ on the product basis derived from $|0\rangle$ and $|S_z, \text{BCS}\rangle$. We write

$$|\mathbf{y}\rangle \equiv |y_1\rangle \otimes ... \otimes |y_N\rangle \tag{S31}$$

in terms of $y_j \in \{-, 0, +\}$. Then, we have

$$\begin{aligned}\Gamma_{j,\sigma}|\mathbf{y}\rangle = (-1)^{\sum_{i<n}(1+\sum_{\sigma'} n_{i,\sigma'})} \\ |y_1\rangle \otimes ... \otimes \Gamma_{j,\sigma}|y_j\rangle \otimes ... \otimes |y_N\rangle .\end{aligned} \tag{S32}$$

Similarly, for the infinite-U Hubbard model

$$\begin{aligned}D_{j,\sigma}|\mathbf{x}\rangle = (-1)^{\sum_{i<n,\sigma'} n_{i,\sigma'}} \\ |x_1\rangle \otimes ... \otimes D_{j,\sigma}|x_j\rangle \otimes ... \otimes |x_N\rangle ,\end{aligned} \tag{S33}$$

where $x_j \in \{\text{vac}_\text{H}, \uparrow_\text{H}, \downarrow_\text{H}, \downarrow\uparrow_\text{H}\}$ and $n_{j,\sigma} = d^\dagger_{j,\sigma}d_{,j\sigma}$. Hence, there is an additional factor of $(-1)^{n-1}$ that needs to be taken into account. With this, the equivalence Eq. (S1) has been established.

Finally, we need to express the spin operators as well as the single-site projector $P_{j,\mathrm{BCS}}$ in terms of the d operators. As shown in the previous section, the spins are now simply the spins in the Hubbard model and hence we have

$$S_j^z \sim \frac{1}{2}\Big(d_{j,\uparrow}^\dagger d_{j,\uparrow} - d_{j\downarrow}^\dagger d_{j\downarrow}\Big) \equiv S_j^z,\ S_j^+ \sim d_{j,\uparrow}^\dagger d_{j,\downarrow} \equiv S_j^+,\ S_j^- \sim d_{j,\downarrow}^\dagger d_{j,\uparrow} \equiv S_j^-, \tag{S34a}$$

$$P_{j,\mathrm{BCS}} \sim \sum_\sigma d_{j,\sigma}^\dagger d_{j,\sigma} \equiv \sum_\sigma n_{j,\sigma}. \tag{S34b}$$

With this we can write the effective model,

$$H_{tJ} = N\Big(V - \frac{3}{4}K\Big) + \sum_j \Bigg\{ - E_{\mathrm{YSR}} \sum_\sigma n_{j,\sigma} + U n_{j,\uparrow} n_{j,\downarrow} + \mathbf{S}_j \cdot J \cdot \mathbf{S}_{j+1} \\ - \tilde{t} \sum_\sigma \Big(d_{j,\sigma}^\dagger d_{j+1,\sigma} + \mathrm{h.c.}\Big) - \tilde{\Delta}\Big(d_{j,\uparrow}^\dagger d_{j+1,\downarrow}^\dagger - d_{j,\downarrow}^\dagger d_{j+1,\uparrow}^\dagger + \mathrm{h.c.}\Big)\Bigg\}, \tag{S35}$$

where $U \to \infty$. This is similar to a $t-J$ model (no double occupation, nearest-neighbor spin interaction), but explicitly includes a pairing term. Furthermore, the spin interaction is not necessarily small and may be ferromagnetic. We hence refer to this model as an extended $t-J$ model. In Eq. 2 in the main text, we replace the $U \to \infty$ Hubbard term by a projection operator $\mathcal{P}$ onto empty and singly-occupied orbitals as customary for $t-J$ models. Finally, note that periodic boundary conditions in the original model translate to periodic boundary conditions in the extended $t-J$ model for N even, and to antiperiodic boundary conditions for N odd (for both hopping and pairing terms). This is due to the factor of $(-1)^1(-1)^N$ arising from products of γ_N and γ_1 and conjugates and corresponds to a π flux threading the infinite-U Hubbard ring for odd-N chains.

C. Spin-orbit coupling in the effective $t-J$ model

We derive the terms in the extended $t-J$ model, when spin-orbit coupling is added to the original model in Eq. (1). We assume that the spin chain is aligned along the x-direction with the normal to the surface pointing along the z-direction. Then, the Rashba spin-orbit term is

$$H_{\mathrm{SOC}} = -it\alpha \sum_j \Big(c_j^\dagger \sigma_y c_{j+1} - \mathrm{h.c.}\Big). \tag{S36}$$

Expressing this in terms of the local Bogoliubov operators given in Eq. (S5) and performing the replacement Eq. (S1), we obtain

$$H_{\mathrm{SOC},tJ} = \alpha \sum_j \Big[-i\tilde{t}\Big(d_j^\dagger \sigma_y d_{j+1} - \mathrm{h.c.}\Big) + \tilde{\Delta}\Big(d_j^\dagger \sigma_0 d_{j+1}^\dagger + \mathrm{h.c.}\Big)\Big]. \tag{S37}$$

Thus, spin-orbit-coupling induces p-wave pairing in the extended $t-J$ model. Note that in the absence of spin order, this does not suffice to open a topological gap. To see this, consider the sum of the hybridization and spin-orbit terms. This may be written as

$$H_{t,tJ} + H_{\mathrm{SOC},tJ} = \sum_j \Big(-d_j^\dagger T_{\mathrm{H}} d_{j+1} + d_j^\dagger \Delta_{\mathrm{H}} d_{j+1}^\dagger + \mathrm{h.c.}\Big), \tag{S38}$$

with $T = \tilde{t}(1 + i\alpha\sigma_y)$ and $\Delta_H = \tilde{\Delta}(1 + i\alpha\sigma_y)(i\sigma_y)$. The tunneling and pairing matrices are phase-locked and no gap opens in the absence of the spin interactions.

D. Spectral function

Tunneling spectroscopy probes the local single-particle spectral function

$$A_{j,\sigma,a}(E) = \sum_\lambda \Big| \langle\lambda|\, \psi_{j,\sigma,a}^\dagger\, |\mathrm{g.s.}\rangle \Big|^2 \delta(E - E_\lambda + E_0), \tag{S39}$$

where we define $\psi_{j,\sigma,a} = (c_{j,\sigma}, c^\dagger_{j,\bar\sigma})_a$ to treat tunneling in and out (or: tunneling of electron and hole) on the same footing ($a = 1 \equiv$ "in", and $a = 2 \equiv$ "out"). Expressing $\psi_{j,\sigma}$ in terms of local Bogoliubov operators and using the mapping to the extended $t - J$ model, we have

$$\psi_{j,\sigma} = \begin{pmatrix} u \\ \sigma v \end{pmatrix} \gamma_{j,\sigma} + \begin{pmatrix} -\sigma v \\ u \end{pmatrix} \gamma^\dagger_{j,\bar\sigma} \sim \frac{(-1)^j}{\sqrt{2}} \left[\begin{pmatrix} \sigma u \\ v \end{pmatrix} d^\dagger_{j,\bar\sigma} + \begin{pmatrix} v \\ -\sigma u \end{pmatrix} d_{j,\sigma} \right]. \tag{S40}$$

Hence, up to a global sign, tunneling in of σ-electron and tunneling out of $\bar\sigma$-electron differ by $u \to \sigma v, v \to -\sigma u$. With this, the spectral function can be expanded as

$$A_{j,\sigma}(E) = \sum_\lambda \Bigg\{ \left| \langle\lambda| \gamma^\dagger_{j,\sigma} |\text{g.s.}\rangle \right|^2 \begin{pmatrix} u^2 \\ v^2 \end{pmatrix} + |\langle\lambda| \gamma_{j,\bar\sigma} |\text{g.s.}\rangle|^2 \begin{pmatrix} v^2 \\ u^2 \end{pmatrix} \tag{S41}$$

$$+ 2uv\, \mathrm{Re}\left[\langle\lambda| \gamma^\dagger_{j,\sigma} |\text{g.s.}\rangle \langle\text{g.s.}| \gamma^\dagger_{j,\bar\sigma} |\lambda\rangle \right] \begin{pmatrix} -\sigma \\ \sigma \end{pmatrix} \Bigg\} \delta(E - E_\lambda + E_0), \tag{S42}$$

or in terms of the extended $t - J$ model

$$A_{j,\sigma}(E) = \frac{1}{2} \sum_\lambda \Bigg\{ \left| \langle\lambda| d^\dagger_{j,\sigma} |\text{g.s.}\rangle \right|^2 \begin{pmatrix} v^2 \\ u^2 \end{pmatrix} + |\langle\lambda| d_{j,\bar\sigma} |\text{g.s.}\rangle|^2 \begin{pmatrix} u^2 \\ v^2 \end{pmatrix} \tag{S43}$$

$$+ 2uv\, \mathrm{Re}\left[\langle\lambda| d^\dagger_{j,\sigma} |\text{g.s.}\rangle \langle\text{g.s.}| d^\dagger_{j,\bar\sigma} |\lambda\rangle \right] \begin{pmatrix} \sigma \\ -\sigma \end{pmatrix} \Bigg\} \delta(E - E_\lambda + E_0). \tag{S44}$$

The states are now to be considered as eigenstates of the extended $t - J$ Hamiltonian H_{eff}. The first and second terms correspond to the electron and hole spectral functions of the extended $t - J$ model, the last corresponds to the spectral function associated with the anomalous Green function. In the main text, we specify to tunneling in and average over spin species, $A_j \equiv \sum_\sigma A_{j,\sigma,\text{in}}$. To obtain the tunneling spectra in Fig. 1 (Fig. 2), we calculate the matrix elements using the exact-diagonalization wave functions and approximate the δ-function as a Gaussian peak with width $\kappa = 0.01t$ ($\kappa = 0.004t$). Finally, note that the spectra are normalized with respect to their individual maximal values $A_{\max} = \max_{E,j} A_j(E)$. Thus, the magnitude should not be compared between different plots.

Using spin-resolved STM, it is in principle possible to measure spin-resolved spectral functions, which are included in Fig. S1, complementing the spin-averaged spectral functions shown in Fig. 1 of the main text.

E. Exact diagonalization

All numerical data in this work are generated by exact diagonalization of Eq. (2) via the Lanczos scheme, setting up the Hamiltonian directly in the locally three-dimensional low-energy-projected Hilbert space (spanned by $|0_j\rangle, |\pm_j\rangle$). We explicitly exploit conservation of fermion parity and of S^z_{tot}. For phase diagrams, we determine the lowest ten eigenvalues and corresponding eigenvectors within each symmetry sector. For spectral functions, we additionally determine the next 300 excited states in the relevant symmetry sector.

II. MEAN-FIELD THEORY OF THE METALLIC FERROMAGNET AND TOPOLOGICAL SUPERCONDUCTIVITY

Topological superconductivity appears in the model of Eq. (1) in the parameter region of the metallic ferromagnet, c.f. main text and Fig. 1 (b). When amending the model by spin-orbit coupling, a p-wave gap can open in this region. As shown in Sec. I C, spin-orbit coupling at the level of the model Eq. (1) introduces a p-wave-pairing term into the extended $t - J$ model, which does not open a gap in the absence of some form of spin order. According to the Mermin-Wagner theorem, there cannot be spin order for isotropic interactions [44]. Hence, we explicitly break the spin rotation symmetries by considering XXZ coupling $J = \mathrm{diag}(J_\perp, J_\perp, J_z)$. Moreover, the spin-orbit coupling, Eq. (S36), breaks the SU(2) spin rotation symmetry down to a U(1) symmetry corresponding to rotations about the

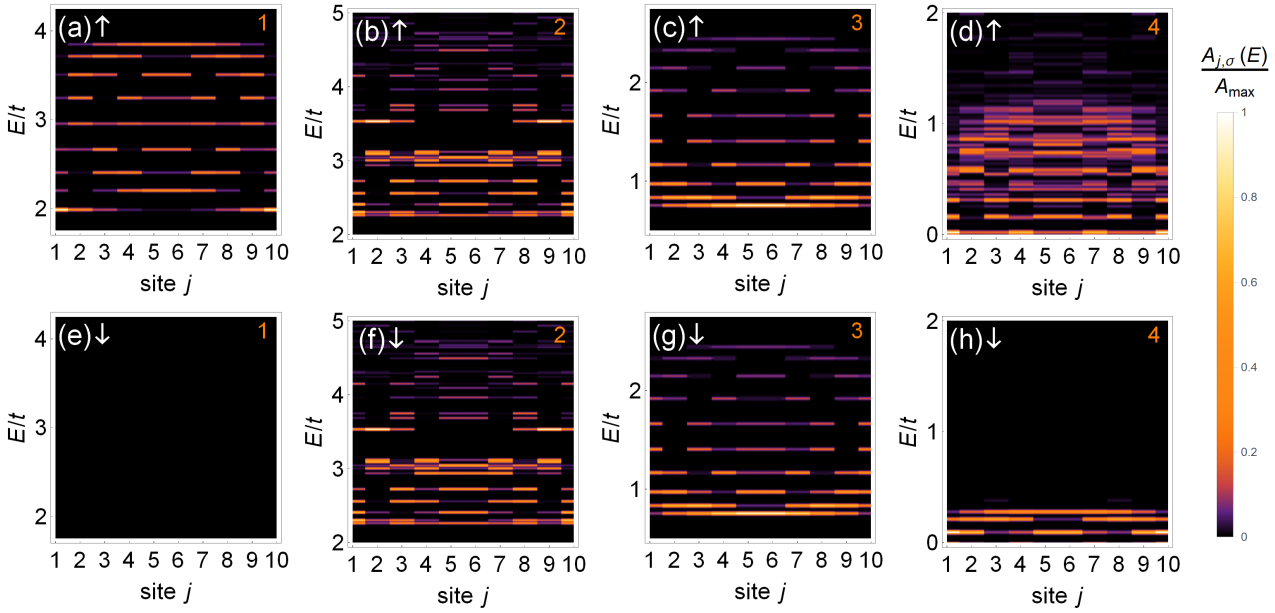

Figure S1. Spin-resolved spectral functions $A_{j,\sigma}(E)$ for the same parameters as in Fig. 1(d)-(g) of the main manuscript. Numbers in the panels refer to the corresponding labels in the phase diagram in Fig. 1(b). A small magnetic field $B_z = -0.001t$ is included to lift the degeneracy in the ferromagnetically ordered phases, such that the ground state is polarized in the spin-down direction. (a)-(d) show spectral functions for $\sigma =\uparrow$, (e)-(h) for $\sigma =\downarrow$ (see also labels shown in panels). The spectra differ between up and down spins only in the ferromagnetically ordered phases (a) vs. (e) and (d) vs. (h). In contrast, the spectra are identical in the $S = 0$ phase, see (b) vs. (f), (c) vs. (g).

y-axis). In the numerics, we specified to the extreme case of an Ising interaction for simplicity, but the arguments below only require $J_z > J_\perp$. Figure S2(a) shows that the qualitative features of the phase diagram for Heisenberg interactions are robust against breaking the spin rotation symmetry. In particular, the ferromagnetic metal phase is maintained. With spin-orbit coupling, see Fig. S2(b), this phase becomes a topological superconductor as we will discuss in more detail below (see also Fig. 2 in the main text).

A. Metallic ferromagnet

The metallic ferromagnet can be accurately described within a simple Hartree-Fock approach. We specify to ferromagnetic XXZ coupling (with $J_z \geq J_\perp$) and focus on states with maximal spin projection. As double occupation is forbidden, we use a spin-polarized Fermi sea as a variational Hartree-Fock ground state,

$$|\mathrm{FS},\uparrow\rangle = \prod_{|k|<k_F} d^\dagger_{k,\uparrow} |\mathrm{vac}\rangle \,, \tag{S45}$$

in terms of $d_{j,\sigma} = \frac{1}{\sqrt{N}} \sum_k d_{k,\sigma} e^{ikj}$ with $k = \frac{2\pi n}{N} \in [-\pi, \pi]$ and $n \in \mathbb{Z}$ (periodic boundary conditions). The Fermi momentum k_F can be viewed as a variational parameter and the number of holes (screened sites) is given by

$$n_{\mathrm{holes}} = N - \sum_{|k|<k_F} \langle \mathrm{FS},\uparrow| \, d^\dagger_{k,\uparrow} d_{k,\uparrow} \, |\mathrm{FS},\uparrow\rangle = N \left(1 - \frac{k_F}{\pi}\right). \tag{S46}$$

Here, the last term on the right hand side takes the thermodynamic limit $N \to \infty$. As the singlet pairing $\tilde{\Delta}$ does not contribute, the Hamiltonian in Eq. (2) implies that this state has energy

$$E_{\mathrm{FS}}(k_F) = \langle \mathrm{FS},\uparrow| \, H \, |\mathrm{FS},\uparrow\rangle = \sum_{|k|<k_F} (-E_{\mathrm{YSR}} - 2\tilde{t}\cos k) + \langle \mathrm{FS},\uparrow| \sum_j \mathbf{S}_j \cdot J \cdot \mathbf{S}_{j+1} \, |\mathrm{FS},\uparrow\rangle \,. \tag{S47}$$

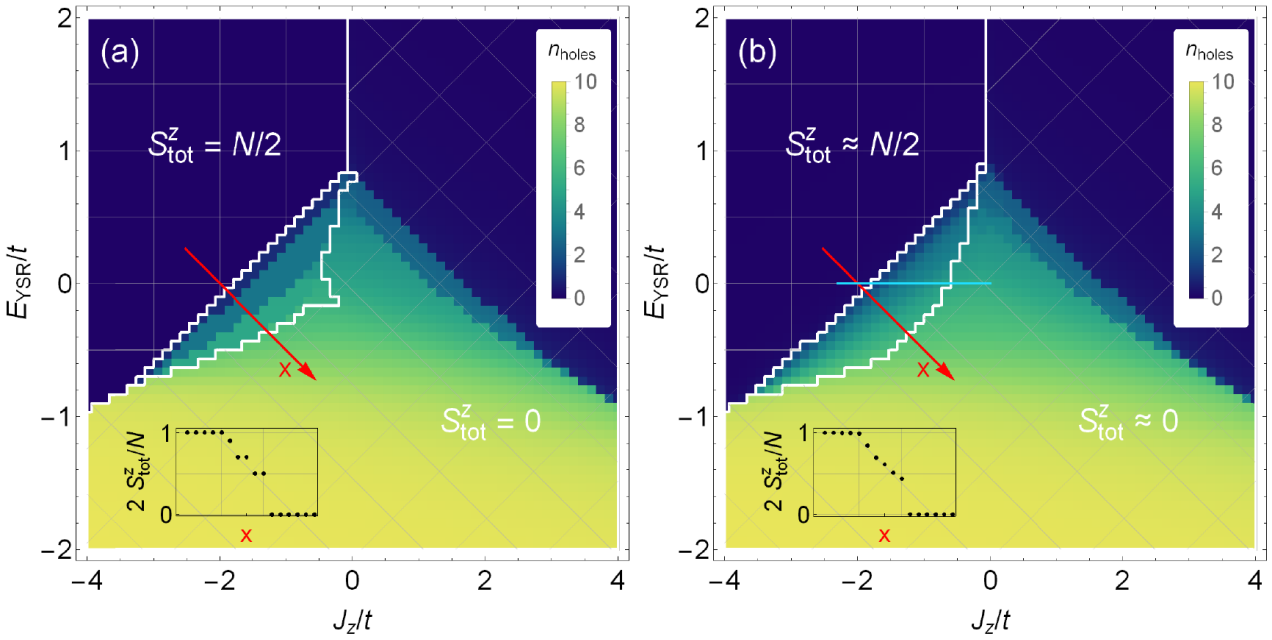

Figure S2. Exact-diagonalization results for $N = 10$ chains with Ising RKKY coupling [$J = \mathrm{diag}(0, 0, J_z)$] and periodic boundary conditions, (a) without and (b) with spin-orbit coupling. In (a), the white lines delineate regions of maximum (minimum) S^z_{tot}. In (b), S^z_{tot} is no longer a good quantum number due to spin-orbit coupling. Here, the white lines delineate regions for which S^z_{tot} is within 0.2 of its extremal values 0 and 5. For both (a) and (b), the rough features of the phase diagram are qualitatively similar to the phase diagram for isotropic RKKY interactions shown in the main text in Fig. 1(b). On the ferromagnetic side $J_z < 0$, (a) exhibits the metallic ferromagnet (enclosed by the white lines). Across this region, the spin is reduced from its maximal value until the phase boundary to the singlet superconductor is reached (inset). The most striking difference in (b) is the breaking of particle number conservation in the ferromagnetic phases (spin-chain phase and metallic ferromagnet), which reflects the triplet contribution to the pairing. The light blue cut corresponds to the parameter range shown in Figs. 2 (a) and (b) of the main text. Parameters: $V = 2\Delta$, $B_z = -10^{-3}t$, (b) $\alpha = 0.25$.

Only the longitudinal exchange coupling J_z contributes to the RKKY interaction and we obtain (for $N \to \infty$)

$$\langle \mathrm{FS}, \uparrow | \sum_j \mathbf{S}_j \cdot J \cdot \mathbf{S}_{j+1} | \mathrm{FS}, \uparrow \rangle = \frac{N J_z}{4\pi^2}(k_F^2 - \sin^2 k_F). \tag{S48}$$

Altogether, we find the energy

$$\begin{aligned} \frac{E_{\mathrm{FS}}(k_F)}{N} &= -\frac{k_F}{\pi} E_{\mathrm{YSR}} - \frac{2\tilde{t}}{\pi} \sin k_F + \frac{J_z}{4\pi^2}\left(k_F^2 - \sin^2 k_F\right) \\ &= \int_{-k_F}^{k_F} \frac{\mathrm{d}k}{2\pi}\, \hat{\xi}(k) - \frac{J_z}{4\pi^2}\left(k_F^2 - \sin^2 k_F\right), \end{aligned} \tag{S49}$$

where we defined the mean-field dispersion

$$\hat{\xi}(k) = -E_{\mathrm{YSR}} - 2\tilde{t}\cos k + J_z\left(\frac{k_F}{2\pi} - \frac{\sin k_F}{2\pi}\cos k\right). \tag{S50}$$

Minimizing the energy with respect to k_F, we find an implicit expression for k_F and hence the number of holes as a function of the YSR energy E_{YSR} and RKKY interaction J_z,

$$0 = \hat{\xi}(k_F). \tag{S51}$$

In particular, this expression with $k_F = \pi$ implies that the transition between the Heisenberg spin chain ($n_{\mathrm{holes}} = 0$) and the metallic ferromagnet occurs for

$$E_{\mathrm{YSR}} = 2\tilde{t} + \frac{J_z}{2}. \tag{S52}$$

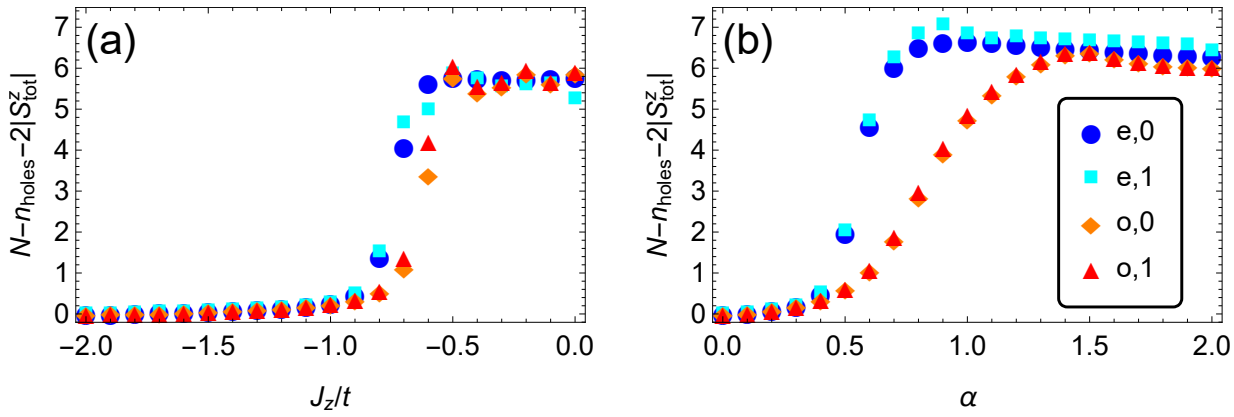

Figure S3. Exact-diagonalization data for the deviation from full spin polarization $N - n_{\rm holes} - 2|S^z_{\rm tot}|$ in a spin-orbit-coupled chain with $N = 12$ sites, with Ising RKKY interactions and open boundary conditions. Blue and cyan markers correspond to two lowest-energy even-parity states (circle, square; labeled by e,0/1), orange and red markers correspond to two lowest-energy odd-parity states (diamond, triangle; labeled by o,0/1). These four states make up the ground-state manifold in Fig. 2(a). The system is approximately spin polarized (deviation from full spin polarization $\simeq 0$) for sufficiently large J_z and sufficiently small α. The latter requirement is due to the tendency of spin-orbit coupling to suppress the spin polarization of the metallic ferromagnet. This delineates the parameter range, for which the spin polarized variational theory developed in this section is adequate. Parameters: $E_{\rm YSR} = 0$, (a) $\alpha = 0.25$, (b) $J_z = -1.25t$. As in Fig. 2, a small magnetic field $B_z = 10^{-3}t$ along the z-direction was added for numerical reasons.

This expression can also be understood by noting that the first hole enters at the top of the band at energy $2\tilde{t}$ and breaks two ferromagnetic bonds. Similarly, we find a transition to a fully screened chain ($k_F = 0$) at

$$E_{\rm YSR} = -2\tilde{t} \tag{S53}$$

for negligible pairing $\tilde{\Delta}$. Nonzero pairing preempts the transition from the metallic ferromagnet into the fully screened chain by the formation of a singlet superconducting phase at a finite density of d fermions. This is not captured by the ansatz Eq. (S45).

B. Topological superconductivity

The metallic ferromagnet serves as a parent state for topological superconductivity, which can develop in the presence of spin-orbit coupling. We choose Rashba spin-orbit coupling as defined in Eq. (S36). To obtain an approximate theory for the topological superconducting phase, we start from the spin-polarized metallic state introduced in the previous section (with k_F determined by $\hat{\xi}(k_F) = 0$) and add p-wave pairing $\Delta_{\rm p}$. We will discuss the precise form of $\Delta_{\rm p}$ below. This assumes that the ground state remains approximately spin polarized in the presence of weak spin-orbit coupling. This is a good approximation for $J_z \lesssim -1$ and $\alpha \lesssim 0.4$ as can be inferred from Fig. S3. The ground-state energy density is

$$\frac{E_{\rm TSC}}{N} = \frac{1}{2}\int_{-\pi}^{\pi}\frac{{\rm d}k}{2\pi}\left[\hat{\xi}(k;k_F) - \sqrt{\hat{\xi}^2(k;k_F) + \Delta_{\rm p}^2(k;k_F)}\right] - \frac{J_z}{4\pi^2}\left(k_F^2 - \sin^2 k_F\right). \tag{S54}$$

and the total spin along the z-direction is

$$S^z_{\rm tot} = \frac{N}{4}\left[1 - \int_{-\pi}^{\pi}\frac{{\rm d}k}{2\pi}\frac{\hat{\xi}(k;k_F)}{\sqrt{\hat{\xi}^2(k;k_F) + \Delta_{\rm p}^2(k;k_F)}}\right]. \tag{S55}$$

The excitation gap is given by

$$E_{\rm gap} = \min_k \sqrt{\hat{\xi}^2(k;k_F) + \Delta_{\rm p}^2(k;k_F)}. \tag{S56}$$

It remains to discuss the p-wave pairing. There are two contributions to $\Delta_{\rm p}(k)$ in the presence of Rashba spin-orbit coupling ($\propto \alpha\sigma_y$): a direct contribution derived in Sec. I C and a contribution mediated by virtual spin flips and singlet pairing. The latter is equivalent to the mechanism by which spin-orbit-coupled nanowires proximity couple to an s-wave superconductor and acquire a p-wave gap (in the strong-field limit). To derive this contribution, we assume a large mean field along the positive z-direction,

$$\frac{J_z S^z_{\rm tot}}{N} \simeq \frac{J_z k_F}{2\pi}. \tag{S57}$$

Treating the pairing terms in perturbation theory and expanding for small $\alpha\tilde{t}/J_z k_F$, we obtain the effective p-wave pairing

$$\Delta_{\rm p}(k;k_F) = 4i\tilde{\Delta}\alpha \sin k\left[1+\frac{2\pi\tilde{t}}{J_z k_F}\cos k\right]. \tag{S58}$$

The results of this section are illustrated in Fig. 2 along with the exact diagonalization data. Panel (a) includes the p-wave gap as determined from Eqs. (S56) and (S58) (black, dot-dashed), while panel (b) includes $|S^z_{\rm tot}|$ and $n_{\rm holes}$ ($= |S^z_{\rm tot}|/2$ within the spin-polarized ansatz) determined from Eqs. (S55). k_F is determined by minimizing the normal state energy, Eq. (S51).

III. CLASSICAL IMPURITY SPINS

For contrast, this section discusses chains of classical impurity spins in more detail. A chain of classical spin impurities $\mathbf{S}_j$ coupled to a superconducting substrate may be described by the Hamiltonian

$$H = H_{\rm sc} + K\sum_j \sum_{\sigma\sigma'} \psi^\dagger_\sigma(\mathbf{R}_j)\mathbf{s}_{\sigma\sigma'}\psi_{\sigma'}(\mathbf{R}_j)\cdot\mathbf{S}_j + E[\{\mathbf{S}_j\}]. \tag{S59}$$

Note that unlike in the quantum case, the $\mathbf{S}_j$ are not operators but act on the electrons merely as local Zeeman fields. We assume that the adatom spins couple antiferromagnetically to the substrate electrons, $K>0$. The configuration of the classical spins minimizes the total energy of the system, and is therefore governed by spin-spin interactions and magnetic anisotropies, which contribute to the energy functional $E[\{\mathbf{S}_j\}]$, as well as the exchange coupling K between adatom spin and substrate electrons.

Figure S4 shows representative results for the phase diagram and the spectral functions for classical spins, assuming the Ising-like RKKY interaction

$$E[\{\mathbf{S}_j\}] = J\sum_j S^z_j S^z_{j+1} \tag{S60}$$

for definiteness. The superconductor is treated within the zero-bandwidth approximation, as we do throughout this paper. Figure S4 assumes $\Delta > V$, while Fig. 1(c) of the main text includes a corresponding phase diagram with $\Delta < V$.

The phase diagrams and the spectral functions are strikingly different compared to the results for quantum spins shown in Fig. 1(b) of the main text. In the classical phase diagram, the metallic ferromagnet with S_z intermediate between $N/2$ and 0 extends out to arbitrarily large and negative values of the RKKY coupling J. In contrast, in the case of quantum spins, the metallic ferromagnet appears only up to a maximal J, beyond which there is a direct transition between the ferromagnetic insulator and the fully screened phase. Moreover, while the phase boundaries are independent of J in the classical phase diagram (except at small J), the phase boundaries are strongly dependent on J in the quantum spin case.

These qualitative differences are rooted in two essential differences between the classical and quantum spin models. First, for a given classical spin configuration $\{\mathbf{S}_j\}$, the adatom chain induces a chain of YSR states. The formation of subgap bands can then be discussed within a (single-particle) Bogoliubov-de Gennes approach. There will be partial occupation of the YSR bands as long as they cross the center of the gap. Since the bandwidth is governed by effective hopping terms (energy scale $\tilde{t}$) and the effective pairing terms (energy scale $\tilde{\Delta}$), while being unaffected by J, the partial-filling phases such as the ferromagnetic metal extend out to arbitrarily large values of J in Fig. S4(a), in sharp contrast to the phase diagram for quantum spins in Fig. 1(b).

Second, classical spins are not screened by the electrons in the superconductor. Although classical spins $\mathbf{S}_j$ bind a local quasiparticle when the YSR energy becomes negative, the adatom spin and the bound quasiparticle form a product state,

$$|\psi\rangle = |\{\mathbf{S}_j\}\rangle\, |\psi_{\rm sc}(\{\mathbf{S}_j\})\rangle\,. \tag{S61}$$

This is in stark contrast to quantum spins, where the screening electrons and the quantum impurity spin form a non-factorizing singlet state. For classical spins, the interaction with other adatom spins will thus remain unaffected when binding or unbinding a quasiparticle. In contrast, spin-$\frac{1}{2}$ quantum spins are effectively screened when binding a quasiparticle. (For higher spins, the adatom spin is reduced by 1/2 with every channel that binds a quasiparticle.) Screening of the adatom spin is the underlying reason for the dependence of the phase boundary in the quantum spin case. While the energy of the unscreened state is lowered by the RKKY interaction, this is not the case for the screened state.

The single-particle nature of the problem as well as the absence of screening for classical spins also implies that the spectral functions are single-particle-band like, see Fig. S4(b)-(g) . This is again in sharp contrast to the result for quantum spins as discussed in the main text. In particular, we find for the case of classical spins that there are no anomalously enhanced or reduced spectral weights at the ends of the chain for ferromagnetic RKKY coupling, and that there is simple band-like behavior for antiferromagnetic RKKY coupling.

For the Ising-like RKKY coupling, we can also make some analytical progress. This energy functional favors spin configurations along the z-axis, so that we can also take the exchange coupling K to be Ising-like. Then, the YSR-energy is

$$E_{\rm YSR} = \sqrt{\Delta^2 + V^2} - \frac{K_z}{4}. \tag{S62}$$

Taking the limit $\Delta, V, K \gg J, t$, the full chain is described by the effective Hamiltonian

$$H_{\rm eff} = P \sum_j \left\{ E_{\rm YSR} \sum_\sigma \gamma^\dagger_{j,\sigma}\gamma_{j,\sigma} - 2\tilde{t} \sum_\sigma \left[\gamma^\dagger_{j,\sigma}\gamma_{j+1,\sigma} + \text{h.c.}\right] + 2\tilde{\Delta}\left[\gamma^\dagger_{j,\uparrow}\gamma^\dagger_{j+1,\downarrow} - \gamma^\dagger_{j,\downarrow}\gamma^\dagger_{j+1,\uparrow} + \text{h.c.}\right] + E[\{\mathbf{S}_j\}] \right\} P, \tag{S63}$$

where P projects onto the low-energy subspace spanned by the states $|S_z, \text{BCS}\rangle$, $|\Uparrow\downarrow\rangle$, and $|\Downarrow\uparrow\rangle$. Figure S4 is obtained by exact diagonalization of this model.

IV. FINITE SIZE EFFECTS IN THE QUANTUM PHASE DIAGRAM

One observes small apparent irregularities in the boundaries of the $S_{\rm tot} = 0$ phase at small $|J|$ in the quantum phase diagram in Fig. 1(b). There are sawtooth-like dents between the ferromagnetic metal and the $S_{\rm tot} = 0$ phase and small regions with $S_{\rm tot} \neq 0$ within the $S_{\rm tot} = 0$ phase. Both of these are due to finite-size effects. The spin structure is depicted in Fig. 1(b) as follows: The $S_{\rm tot} = 0$ phase is indicated by a tilted mesh, while the $S_{\rm tot} = N/2$ phase is indicated by a vertical/horizontal mesh. Boundaries of these phases are indicated by thick white lines. The ferromagnetic metal phase has $0 < S_{\rm tot} < N/2$ as indicated by the absence of a mesh.

Consider first the sawtooth-like dents between the ferromagnetic metal and the $S_{\rm tot} = 0$ phase. These may be understood in terms of the infinite-U Hubbard model, which our model maps to for $J = 0$ and $\tilde{\Delta} = 0$. The Bethe-ansatz solution for the infinite-U Hubbard model has a straightforward interpretation in terms of spin charge separation [42]. The eigenfunctions are comprised of an effectively spinless Slater determinant of plane-wave states with momenta $\{k_i\}$ and a spin wave function. The latter carries a spin-crystal momentum Λ, which depends on the spin configuration: $\Lambda = 0$ for $S_{\rm tot} = Q/2$, and $\Lambda = \pi$ for $S_{\rm tot} = 0$ (here, $Q = \sum_i n_i$ is the total charge). Then, the momenta satisfy the boundary condition

$$e^{iNk_i} = e^{i\Lambda} \tag{S64}$$

and the total energy takes the free fermion form

$$E(\{n_i\}) = -2\tilde{t} \sum_i n_i \cos k_i. \tag{S65}$$

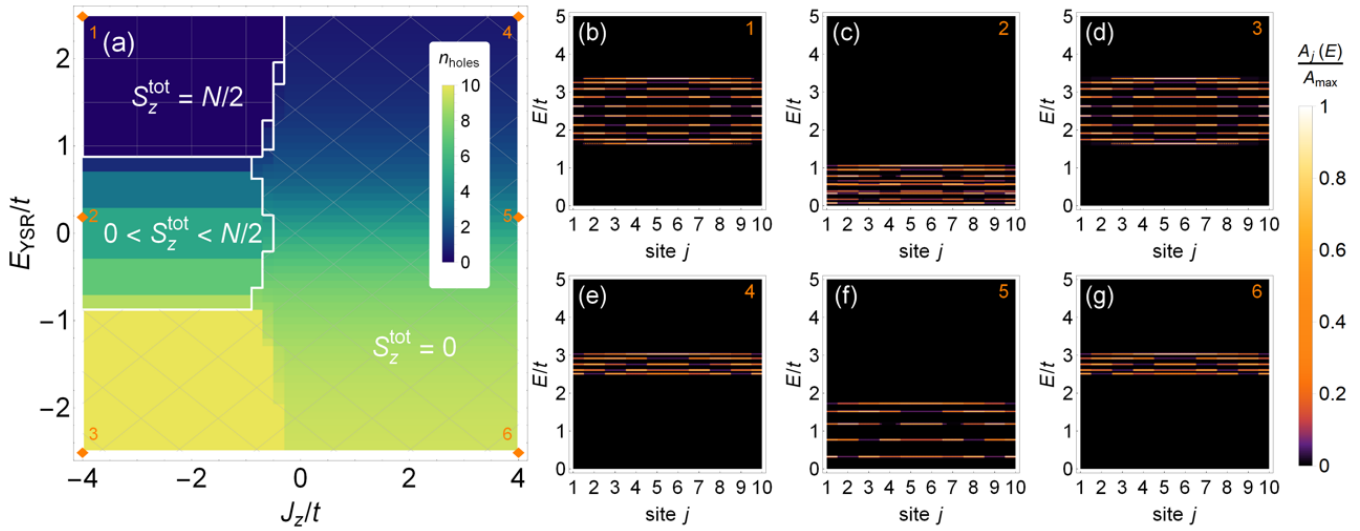

Figure S4. Exact diagonalization data for the model in Eq. (S63) with classical spin and Ising RKKY coupling ($\Delta = 2V$, $N = 10$; Fig. 1(c) in the main text shows data for $V = 2\Delta$). (a) Phase diagram analogous to Fig. 1(b) in the main text. For $\Delta > V$, pairing dominates over kinetic energy, so that the antiferromagnetic phase extends into the $J < 0$ region at small $|E_{\rm YSR}|$. (b - g) Tunneling spectra for $(E_{\rm YSR}, J_z) \in \{(2.5, -4), (0.2, -4), (-2.5, -4), (2.5, 4), (0.2, 4), (-2.5, 4)\}$ [orange diamonds in (a)]. As opposed to the spectral functions for quantum spins, all spectra are single-particle like with $\sim N$ contributing states. Again opposed to quantum spins, the spectral functions are symmetric in energy under $E_{\rm YSR} \to -E_{\rm YSR}$. For ferromagnetic RKKY interaction, (b-d), pairing is ineffective and one observes simple particle-in-a-box states with band-width $4\tilde{t}$. In (c) the band is partially filled and thus the hole and electron spectra overlap. For antiferromagnetic RKKY coupling, (e-g), tunneling is frustrated, but there is still dispersion due to the intersite nature of pairing, with bandwidth $\sim \tilde{\Delta}$.

Hence, for $S_{\rm tot} = 0$, the allowed momenta correspond to antiperiodic boundary conditions, whereas for $S_{\rm tot} = Q/2$, the allowed momenta correspond to periodic boundary conditions. To minimize the kinetic energy, an even number of fermions favors antiperiodic boundary conditions (for which $k = 0$ is not an allowed momentum) and hence a singlet-spin configuration, while an odd number favors periodic boundary conditions (where $k = 0$ is an allowed momentum) and hence a maximum-spin configuration. This is illustrated in Fig. S5. For finite system sizes, a minimal RKKY coupling is needed to overcome this finite-size effect and one observes a shift of the phase boundary of the $S_{\rm tot} = 0$ phase towards more negative J, whenever $E_{\rm YSR}$ is such that the system favors an even number of fermions. (Remember that $E_{\rm YSR}$ effectively acts as a chemical potential for the fermions.)

Importantly, this behavior is also observed in the absence of pairing and hence should not be confused with the competition between the ferromagnetic metal and singlet superconductor phases discussed in the main text. The latter is clearly not a finite-size feature. Pairing further stabilizes the $S_{\rm tot} = 0$ phase for any number of fermions. This explains that the $S_{\rm tot} = 0$ phase preempts the ferromagnetic metal phase at small, but negative J, regardless of the value of $E_{\rm YSR}$.

Finally, consider the small islands of $S_{\rm tot} \neq 0$ for $J > 0$, surrounded by the $S_{\rm tot} = 0$ phase. In these regions, the ground state has an odd number of fermions and hence at least $S_{\rm tot} = 1/2$. In thermodynamic limit this is irrelevant as the spin-density still vanishes.

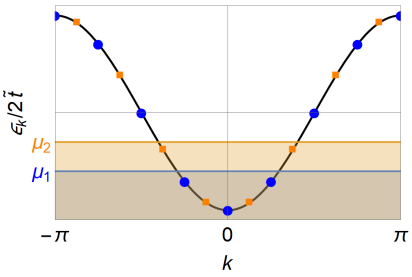

Figure S5. Infinite-U Hubbard model. Depending on the spin state, the effective free fermion states obey periodic or antiperiodic boundary conditions. If the chemical potential is such that it is beneficial to host an even number of electrons (orange shading) antiperiodic boundary conditions are favorable. If an odd number of electrons is preferred, periodic boundary conditions are favorable.